An Ambiguity-Free Depth Detection Method for Wireless Capsule Endoscopy by Combining Frequency Locking and Signal Strength Tracking of Self-Injection-Locked Radars

Jyun-Yan Lai[#1], Hao-Ping Li[#], Sheng-Fuh Chang[#$], Chia-Chan Chang[#$], Shih-Cheng Lin[#$]
[#]Department of Electrical Engineering, National Chung Cheng University, Taiwan
[$] Department of Communications Engineering, National Chung Cheng University, Taiwan
[1]jyunyan_lai@alum.ccu.edu.tw

***Abstract*— This paper presents a novel depth detection method without range ambiguity for localizing wireless capsule endoscopy (WCE). The WCE may locate in a several-wavelength depth from the skin during its entire traveling path of the gastrointestinal (GI) tract. This work introduces a range ambiguity problem when the phase of the RF signal is utilized to estimate the target distance in conventional continuous-wave Doppler radars or self-injection-locked (SIL) radars. To solve this problem, we propose a new SIL-based radar with both functions of frequency locking and signal-strength tracking of the received signal. The measurement results show that the average depth error is 1.4 mm, and the maximal error is 3.3 mm for the target in a depth range of 10-50 mm. This demonstrates that the phase wrapping can be effectively unwrapped so that the implant depth can be unambiguously determined over a long depth range.**

***Keywords*—self-injection locked, implant detection, biosensor, ambiguity.**

I. Introduction

Wireless capsule endoscopy (WCE) is a non-invasive diagnostic device for visualizing the human gastrointestinal (GI) tract [1]. When the WCE moves with the peristalsis of the gastrointestinal tract, the off-body interrogator receives the captured image signal emitted by the endoscope. Knowing the exact position of the WCE is crucial to physicians in identifying the position of detected gastrointestinal diseases.

Various WCE localization techniques have been introduced, including image-based localization [2], permanent-magnet-based localization [3], coil-based localization [4], the RF localization techniques [5]-[7]. The image-based localization technique estimates the orientation of the capsule by analyzing the change in the features of consecutive recorded images. However, this method has restrictions due to image distortion and discontinuity. For the permanent-magnet-based method, the permanent magnet is placed in the WCE, and an array of magnetic sensors surrounding the body are used to detect the magnetic field intensity to determine the position of the target.

The RF-based localization requires RF interrogators surrounding the human body to receive the signal emitted from the WCE in the organ. Their operation frequency is restricted in the industrial scientific and medical (ISM) band, from 300 MHz to 3 GHz. The trilateral or triangular localization principle is applied to determine the WCE position based on the measured radio signal strength (RSS), time of arrival (TOA), and time difference of arrival (TDOA) [5]-[7].

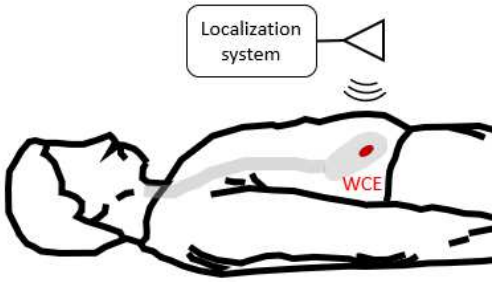

Fig. 1. Scenario of the proposed localization system

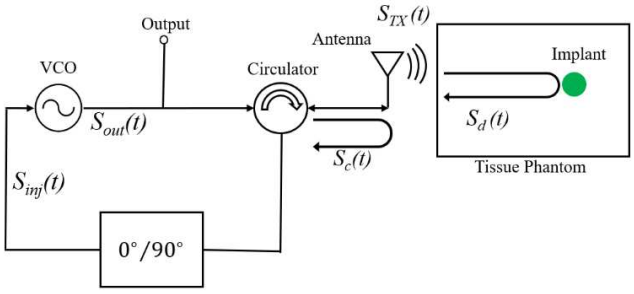

Fig. 2. Block diagram of the proposed SILO system.

For the RF-based localization technique, the WCE may locate in a several-wavelength depth from the skin during the entire path traveling from the esophagus to the colon. This work introduces a range ambiguity problem when the phase of the RF signal is utilized to estimate the target distance when realizing an RF interrogator with high-sensitivity continuous-wave localization radars or self-injection-locked (SIL) radars [8]-[10]. The ambiguous distance results in a significant error in wavelengths.

To address this problem, a new localization method is proposed, which combines the self-injection frequency locking and signal strength tracking of the backscattered signal from the WCE in SIL radars.

II. Phase Tracking and Unwrapping

The range ambiguity resulted from the phase wrapping when the electromagnetic wave propagates across every 2π radians, corresponding to a wavelength. Hence the phase of the received signal scattered from the target is treated first.

Table 1. RF components in the developed radar

Component	Specification
SILO	Tuning range: 927-1110 MHz Output power: 4.7 dBm Phase noise (Injection state): -96.90 dBc/Hz @1 MHz offset
On-body antenna	Return loss > 10 dB (700 – 1200 MHz)
Circulator	Return loss: > 19 dB Insertion loss: < 0.5 dB Isolation: >20 dB

A. Phase of the Received Signal

The block diagram of the SIL radar is plotted in Fig. 2, where the radar consists of a SIL oscillator (SILO), an on-body antenna, a circulator, and a phase shifting component. Table 1 summarizes the specifications of the RF components of the radar. The signal $S_{out}(t)$ from the SILO, having an instantaneous frequency of $\omega_{osc}(t)$, is transmitted upon the abdomen. This signal will be partially reflected by the air-skin interface and partially transmitted into the stomach. The reflected signal $S_d(t)$ from the implant and the skin-reflected clutter $S_c(t)$ will both be injected into the SILO.

When the SILO reaches a new injection-lock state, the instantaneous frequency $\omega_{out}(t)$ of the output signal $S_{out}(t)$, becomes below for the phase shifting component is converted into 0° and 90° state [10]:

$$\omega_{out,0} \approx \omega_{osc,o} - \omega_{LR,d}\sin\phi_d - \omega_{LR,c}\sin\phi_c\,, \qquad (1)$$

$$\omega_{out,90} \approx \omega_{osc,o} + \omega_{LR,d}\cos\phi_d + \omega_{LR,c}\cos\phi_c\,. \qquad (2)$$

In (1) and (2), $\omega_{LR,d}$ and $\omega_{LR,c}$ denote the lock-in ranges of the SILO, corresponding to the backscattered signal and the clutter signal, respectively:

$$\omega_{LR,d} = \frac{\omega_{osc,o}}{2Q}\frac{A_{inj,d}}{A_{osc,o}} \text{ and } \omega_{LR,c} = \frac{\omega_{osc,o}}{2Q}\frac{A_{inj,c}}{A_{osc,o}}\,, \qquad (3)$$

where $\omega_{bsc,o}$, and Q are the free-running frequency and the quality factor of the oscillator, respectively. The phase terms ϕ_c and ϕ_d in (1) and (2) represent the phase difference of $S_c(t)$ and $S_d(t)$ with respect to $S_{out}(t)$. The ϕ_d is of particular interest since it is the actual phase information of the EM wave traveling from the skin to the implant in deep tissue.

To extract the desired ϕ_d from (1) and (2), a clutter elimination procedure is taken first by measuring the SILO output frequency without the presence of the implant. Then, the ϕ_d can be obtained by arctangent demodulation, shown as below

$$\phi_d = -4\pi\frac{x}{\lambda_d} + \phi_0 \mod 2\pi\,, \qquad (4)$$

where x is the depth of the implant from the skin and λ_d denotes the wavelength in the body, ϕ_0 represents the phase delay from the radar circuits, and 'mod 2π' means the 2π phase wrapping.

Eq. (4) has been shown to be very accurate in determining heartbeat and breath rates. However, for the depth detection of the target placed in several wavelengths deep below the abdomen skin, phase wrapping occurs, which results in a large error in depth estimation.

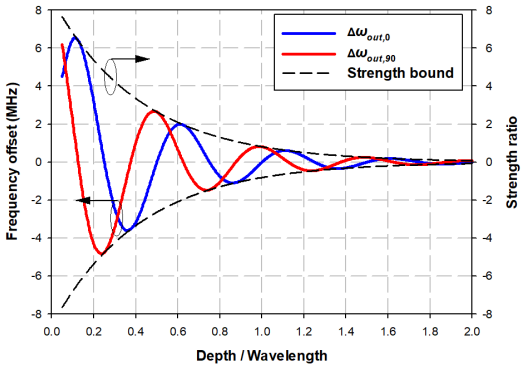

Fig. 3. The frequency offset and the normalized signal strength of the SILO when the implant locates at different depths in the stomach. $f_{osc,o}$=915 MHz, Q=10, $A_d / A_{osc,o}$=0.3.

B. Phase Un-Wrapping by Using Decayed Signal Strength

By further examining (1), the SILO output frequency $\omega_{out}(t)$ depends on two factors. The first factor is the phase term ϕ_d, which is used to estimate the target depth in (4), which suffers from the phase wrapping problem. The second factor is the signal strength through the lock-in range $\omega_{LR,d}$. Although this factor is usually not paid attention to, it will be used to solve the phase wrapping problem, explained below.

When the WCE stays in the stomach, the abdomen, including multiple layers of skin, fat, and muscle, can be characterized by an effective constant of 54.9 and a conductivity of 1.07 S/m [11]. The abdomen is highly conducive at 915 MHz. Therefore, the wave propagating inside the abdomen is more like a decayed sinusoidal wave. As a consequence, the injection signal, corresponding to the desired target backscattered signal, can be written as

$$S_{inj,d}(t) = A_d e^{-2\alpha x}\cos\left(\omega_{osc}t - 4\pi x/\lambda_d + \phi_o\right). \qquad (5)$$

By substituting (3) and (5) into (1) and (2), the fractional output frequency of the SILO can be obtained as below, where the clutter signal is assumed to be cleanly eliminated,

$$\Delta\omega_{out,0} = -\frac{\omega_{osc,o}}{2Q}\frac{A_d e^{-2\alpha x}}{A_{osc,o}}\sin\left(-\frac{4\pi}{\lambda_d}x\right), \qquad (6)$$

$$\Delta\omega_{out,90} = +\frac{\omega_{osc,o}}{2Q}\frac{A_d e^{-2\alpha x}}{A_{osc,o}}\cos\left(-\frac{4\pi}{\lambda_d}x\right). \qquad (7)$$

Eq. (6) and (7) imply that the output frequency offset of the SILO has a decayed sinusoidal/co-sinusoidal relationship with the implant depth, as plotted in Fig. 3. The frequency offset value has a spatial period of 2.21 cm, $0.5\lambda_d$ at 915 MHz, which means the target depth cannot be uniquely determined by detecting the SILO output frequency. Each $0.5\lambda_d$ is a distance ambiguity zone.

When we examine the frequency offset waveforms depicted in Fig. 3 more closely, the frequency shift is decayed with the target depth as well, which indicates the frequency shift is influenced by the signal strength. Therefore, the signal strength

can be used to identify the correct zone where the actual output frequency belongs.

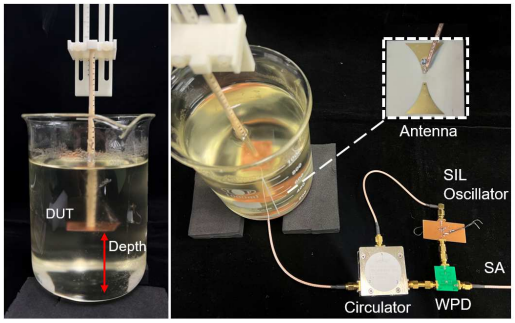

Fig. 4. Photograph of the implemented SIL radar.

III. Experimental Results

Fig.4 shows the photograph of the implemented 915 MHz SIL radar. The SILO transmits the 915 MHz CW signal to the on-body antenna, which is placed at the bottom of the jig. The jig is filled with a carefully prepared solution as a tissue phantom. The phantom is measured to have a dielectric constant of 55.6 and a conductivity of 1.01 S/m, which is similar to the electric characteristic of muscle. A 3×3 cm^2 metal plate is put in the tissue phantom. The phase shifting component is switched to 0° and 90° alternatively to dictate the I- and Q-waveform of the received signal.

To calibrate the ϕ_0 in (4) and obtain a reference point for signal strength to (6) and (7), the location at 1 cm below the skin is taken as the calibration point. Fig. 5 shows the output frequency offset of the I-waveform and Q-waveform with respect to the target depth. The phase wrapping phenomenon is clearly seen, which has three ambiguity zones over the 10-50 mm range, with each zone of 11.4 mm. This measured ambiguity zone agrees very well with the theoretical prediction in Fig. 3. By substituting the measured output frequency into (4), (6), and (7) and comparing the frequency offset to the calibration point, the target depth can be obtained, as shown in Fig. 6. The average depth error is 1.3 mm with a maximum error of 3.3 mm over 10 mm to 50 mm. Our proposed method has the best accuracy compared to the state-of-the-art works, as shown in Table 2.

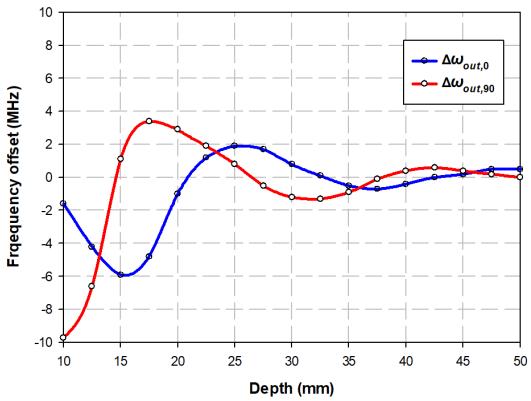

Fig. 5. Measured output frequency offset (dotted) of 915 MHz SIL radar with respect to the target depth.

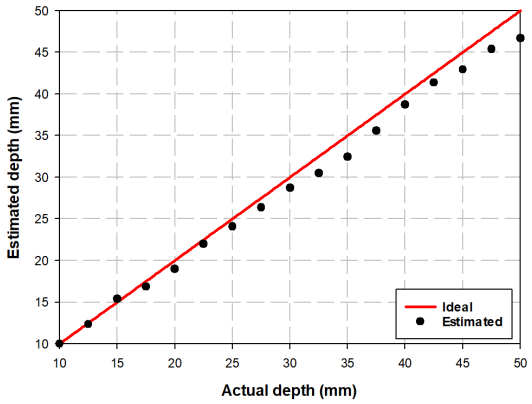

Fig. 6. The estimated depth from the measured output frequency and signal strength.

Table 2. Comparison of the proposed method with the state-of-the-art WCE localization techniques.

Ref.	Technique	Localization Dimension	Localization Error
This work	RF/TOA&RSS	1D	1.3 mm (average)
[3]	permanent magnet/RSS	3D	10 mm (average)
[4]	Coil/RSS	3D	13 mm (worst)
[5]	RF/RSS	3D	9.4 mm (average)

IV. Conclusion

This paper presents a 915 MHz SIL radar for accurately detecting the depth of WCE. For conventional CW or SIL radars, a severe range ambiguity problem occurs due to the phase wrapping effect when the WCE moves in the deep organs. To solve this problem, both the phase and strength of the received signal are detected from the self-injection locked radar. The signal strength is used to determine the correct depth zone, and the phase is used to estimate the actual implant depth. A 915 MHz CW SIL radar is implemented. The measurement results show that an average depth error of 1.35 mm is achieved for the implant moving from 10 mm to 50 mm. This confirms the accuracy of the proposed method and demonstrates the great potential for applying this method to a real-time three-dimension localization system.

Acknowledgment

This work was supported in part by the Ministry of Science and Technology of Taiwan under Grants MOST 109-2221-E-194-002-, MOST 110-2221-E-194-014-.

References

[1] N. Dey, A. S. Ashour, F. Shi and R. S. Sherratt, "Wireless Capsule Gastrointestinal Endoscopy: Direction-of-arrival estimation based localization survey," *IEEE Reviews in Biomedical Engineering*, vol. 10, pp. 2-11, 2017.

[2] S D. K. Iakovidis, G. Dimas, A. Karargyris, F. Bianchi, G. Ciuti, and A. Koulaouzidis, "Deep endoscopic visual measurements," *IEEE J. Biomed. Health Informat.*, vol. 23, no. 6, pp. 2211–2219, Nov. 2019.

[3] G. Shao, Y. Tang, L. Tang, Q. Dai and Y.-X. Guo, "A novel passive magnetic localization wearable system for wireless capsule endoscopy," *IEEE Sensors J.*, vol. 19, no. 9, pp. 3462-3472, 1 May, 2019.
[4] S. R. Khan, S. Mitra and M. P. Y. Desmulliez, "Use of a 3-D wireless power transfer technique as a method for capsule localization," *IEEE Access*, vol. 9, pp. 131685-131695, 2021.
[5] M. Barbi, C. Garcia-Pardo, A. Nevarez, V. Pons Beltran, and N. Cardona, "UWB RSS-based localization for capsule endoscopy using a multilayer phantom and in vivo measurements," *IEEE Trans. Antennas Propag.*, vol. 67, no. 8, pp. 5035–5043, Aug. 2019.
[6] M. Pourhomayoun, Z. Jin, and M. L. Fowler, "Accurate localization of in-body medical implants based on spatial sparsity," *IEEE Trans. Biomed. Eng.*, vol. 61, no. 2, pp. 590–597, Feb. 2014.
[7] A. Nafchi, S. T. Goh, and S. R. Zekavat, "Circular arrays and inertial measurement unit for DOA/TOA/TDOA-based endoscopy capsule localization: Performance and complexity investigation," *IEEE Sensors J.*, vol. 14, no. 11, pp. 3791–3799, Nov. 2014.
[8] P. -Y. Lyu, P. -C. Lo, S. -F. Chang, S. -C. Lin and C. -C. Chang, "A high range-accuracy interferometry radar for very small transponder positioning," *2019 16th European Radar Conference (EuRAD)*, pp. 89-92, 2019.
[9] F.-K. Wang, P.-H. Juan, S.-C. Su, M.-C. Tang and T.-S. Horng, "Monitoring displacement by a quadrature self-injection-locked radar with measurement- and differential-based offset calibration methods," *IEEE Sensors J.*, vol. 19, no. 5, pp. 1905-1916, March, 2019.
[10] M. Scherhäufl, F. Hammer, M. Pichler-Scheder, C. Kastl and A. Stelzer, "Radar distance measurement with viterbi algorithm to resolve phase ambiguity," *IEEE Trans. Microwave Theory Tech.*, vol. 68, no. 9, pp. 3784-3793, Sept. 2020.
[11] D. L. Means and K. W. Chan., "Evaluating compliance with FCC guidelines for human exposure to radiofrequency electromagnetic fields," *OET bulletin*, vol. 65, no. 10, 1997.